# Supporting Information

## Rational synthesis of carbon-rich hollow carbon nitride spheres for photocatalytic $H_2O_2$ production and Cr (VI) reduction

**Yong Hu, [a] Zhenchun Yang, [b] Dandan Zheng, *[a] Wandong Xing*[b], and Guigang Zhang***

[a.] College of Environment and Safety Engineering, Fuzhou University, Fuzhou, 350108, PR China
[b.] State Key Laboratory of Photocatalysis on Energy and Environment, College of Chemistry, Fuzhou University, Fuzhou, 350108, PR China

## 1. Characterization

The morphology of the samples was characterized with field emission scanning microscopy (SU-8010, Hitachi) and TEM FEI (Tecnai 20 FEG). The powder X-ray diffraction patterns were obtained with a Bruker D8 Advance diffractometer with Cu-Kα1 radiation (λ = 1.5406 Å). Fourier transform infrared (FT-IR) spectroscopy was performed on a Nicolet IS50 FITR spectrometer with a scanning range of 4000 to 500 $cm^{-1}$ at room temperature. The X-ray photoelectron spectroscopy (XPS) measurements were performed in a Thermo ESCALAB250 instrument with a monochromatic Al-Kα line source (200 W). Nitrogen adsorption-desorption isotherms were carried out on a Micromeritics ASAP3020 specific surface area and porosity analyzer at 77.2K. The UV-Vis diffuse reflectance spectroscopy (DRS) was performed on a Varian Cary 500 scanning UV-Vis system. Photoluminescence (PL) spectra were performed in a Horiba Fluorolog-3 fluorescence spectrometer at the excitation wavelength of 365 nm. Electron paramagnetic resonance (EPR) spectra were recorded using a Bruker model A300 spectrometer. Kelvin probe force microscopy (KPFM) measurements was completed at SPM-9700 surface probe system (Shimadzu, Japan).

## 2 Photocatalytic activity tests

### 2. 1 Photocatalytic $H_2O_2$ production

An amount of 25 mg of photocatalyst was added to 50 mL of an aqueous solution containing 10 vol% ethanol and then dispersed by sonication for 10 min. The photoreactor was irradiated with a 300w xenon lamp at 25 ℃ and 1 atm, and oxygen was supplied by an oxygen bag. The suspension was sampled at set time intervals for analyzing $H_2O_2$ production properties. The DPD/POD method and titanium sulfate method reported elsewhere were used to determine low and high concentrations of hydrogen peroxide, respectively. The DPD/POD method is based on the horseradish peroxidase (POD) catalyzed oxidation of N, N-diethyl-phenylenediamine (DPD) by hydrogen peroxide, and the concentration of hydrogen peroxide was determined by UV spectrophotometry at 552 nm. The titanium sulfate method utilizes titanium sulfate and hydrogen peroxide to form a yellow titanium peroxide complex, and the concentration of hydrogen peroxide is measured

by UV spectrophotometer at 407nm. Calibration curves were prepared separately using a series of $H_2O_2$ solutions of known concentration.

2. 2 Photocatalytic reduction of Cr (VI)

An amount of 25 mg of photocatalyst was added to 50 mL of an aqueous solution containing 10 vol% ethanol and then dispersed by sonication for 10 min. The photoreactor was irradiated with a 300w xenon lamp at 25 ℃ and 1 atm, and the reduction performance of Cr (VI) was determined under nitrogen and air, respectively. The suspension was sampled at set time intervals, and the photocatalytic Cr (VI) reduction rate was determined by the diphenylcarbazide method. Diphenylcarbazide spectrophotometry is a method that utilizes acidic conditions to generate a purple-red complex between hexavalent chromium ions and diphenylcarbazide, and determines the content of Cr (VI) by UV spectrophotometry at 554nm.

2. 3 Apparent quantum yield（AQY）

12.5 mg of catalyst was dispersed in 25 ml of aqueous ethanol (10 vol.%) and ultrasonically dispersed for 10 min. The dispersed mixture was placed on a stirrer with an oxygen bag to keep the catalyst suspended in the solution. Cover the reactor with a fixed-area piece of tin foil, reserving only a 9 $cm^2$ window. The reaction solution was irradiated with different wavelengths of light through a reserved window for 15 min, and a certain amount of the reaction solution was taken and filtered through a 0.22um polytetrafluoroethylene filter to detect the concentration of hydrogen peroxide. The apparent quantum yield was then calculated using the following equation.

The apparent quantum yield (AQY) is calculated in Equation:

$$AQY = \frac{2 \times Amount\ of\ H_2O_2 \times E_\lambda \times N_A}{P_{\lambda \times a \times t}} \times 100\%$$

$P_\lambda$ is the optical power density irradiated to the reactor surface (mW $cm^{-2}$); $a$ is the open window area of the reactor (0.0001 $m^2$); $t$ is the light irradiation time (s); $E_\lambda$ is the energy of photons in each band; $N_A$ is Avogadro's constant ($6.02 \times 10^{23}$); $A$ is the absorbance of the mixture at different wavelengths.

## 3. Photoelectrochemical tests

Electrochemical measurements were recorded by a BioLogic VSP-300 electrochemical system with a three-electrode system. The Ag/AgCl electrode (3 M KCl) is used as a reference electrode, and a Pt electrode is used as a counter electrode. For the working electrode, the fluorine-doped tin oxide (FTO) glass was cleaned by ultrasonication in ethanol for 10 min and then dried. The conductive surface of the FTO glass was covered with white tape, leaving only the fixed area. A 5 mg sample was sonicated for 1 h to

disperse in the suspension of 0.3 mL ETOH and 0.1 mL $H_2O$, and then the mixture was dropped on the exposed FTO conductive surface. After natural drying in air, the working electrode was further dried at 100 °C for 2 h. The tape was then removed and the uncoated portion was coated with epoxy resin. A 0.2 mol·$L^{-1}$ $Na_2SO_4$ aqueous solution (pH=6.8) was chosen as the supporting electrolyte.

**Table S1.** Chemical component analysis of the samples by X-ray photoelectron spectroscopy

| Sample | C-N=C (%) | C-C (%) | C-NH/C=N (%) | C (%) | N (%) | C/N (%) |
|---|---|---|---|---|---|---|
| $HCNS_{G30}$ | 51.35 | 35.25 | 9.39 | 36.36 | 42.8 | 0.849 |
| HCNS | 68.2 | 27.01 | 4.79 | 32.9 | 53.3 | 0.617 |

**Table S2.** Chemical component analysis of the samples by elemental analysis

| Sample | C (%) | N (%) | H (%) | C/N (%) |
|---|---|---|---|---|
| $HCNS_{G30}$ | 52.81 | 31.48 | 2.99 | 0.596 |
| HCNS | 55.82 | 31.57 | 2.59 | 0.565 |

**Table S3**. Summary of $H_2O_2$ production over various photocatalysts.

| Photocatalyst | Stability | Quantum yields | Scalability | $H_2O_2$ production $\mu mol \cdot h^{-1} \cdot g^{-1}$ | Reference |
|---|---|---|---|---|---|
| C, O co-doped polymeric g-$C_3N_4$ | 6 times Cycle | 420nm 7% | $CO_2$ reduction | 120 | 1 |
| P,N Co-Dopedg-C3N4 HollowSphere | 11 times Cycle | - | - | 4568 | 2 |
| Porous carbon-doped g-$C_3N_4$ | 5 times Cycle | - | BPA Degradation | 748.8 | 3 |
| C-doped g-$C_3N_4$ | 5 times Cycle | - | - | 3524.4 | 4 |
| Defected carbon doped g-$C_3N_4$ | 4 times Cycle | - | 4-CP Degradation | 179.82 with 2h in pure water | 5 |
| CCN-MCAU-DMSO | 5 times Cycle | - | - | 1119.37 | 6 |
| CCN-SA/T-KF | 5 times Cycle | - | - | 1603 | 7 |
| CNT | 4 times Cycle | 400nm 22% | tetracycline degradation | 2480 | 8 |
| $HCNS_{G30}$ | 5 times Cycle | 400nm 12.8 % and 420nm 4.1% | Cr（VI） Reduction | 8811.2 | This Work |

**Table S4**. summary of Cr(VI) reduction over various photocatalysts

| Photocatalyst | Stability | Quantum yields | Scalability | Cr(VI) reduction Efficiency | Reference |
|---|---|---|---|---|---|
| $Bi_{12}O_{17}Cl_2$/Zn-HMT | 5 times cycle | - | TC-HCl degradation | 150 min 65% | 9 |
| CdS/HPA-2/g-$C_3N_4$ | 4 times cycle | - | RhB degradation | 20 min 100% | 10 |
| $In_2S_3$/$Gd_2O_3$ | 5 times cycle | - | OTC degradation | 55 min 96.3% | 11 |
| rGO@ZnAlTi-LDO | - | - | TC-HCl degradation | 210min 80% | 12 |
| Amine-CdS/$MoO_3$ | 5 times cycle | - | Hydrogen Production | 40 min 74% | 13 |
| *N*-deficient g-$C_3N_4$ | - | - | Hydrogen Production | 150 min 75% | 14 |
| g-$C_3N_4$/BP/$MoS_2$ | 5 times cycle | - | Hydrogen Production | 25min 100% | 15 |
| CdS/CdO@Au | 5 times cycle | - | Hydrogen Production | 20 min 98% | 16 |
| CoSx/CdS | 5 times cycle | - | - | 30min 99.8% | 17 |
| $MoO_3$@ZIF-8 | 4 times cycle | - | - | 40 min 96% | 18 |
| g-$C_3N_4$@MIL-53(Fe) | 4 times cycle | - | - | 180min 99% | 19 |

| | | | | | |
|---|---|---|---|---|---|
| $HCNS_{G30}$ | 5 times Cycle | 400nm 12.8 % and 420nm 4.1% | $H_2O_2$ production | 10min 100% | This Work |

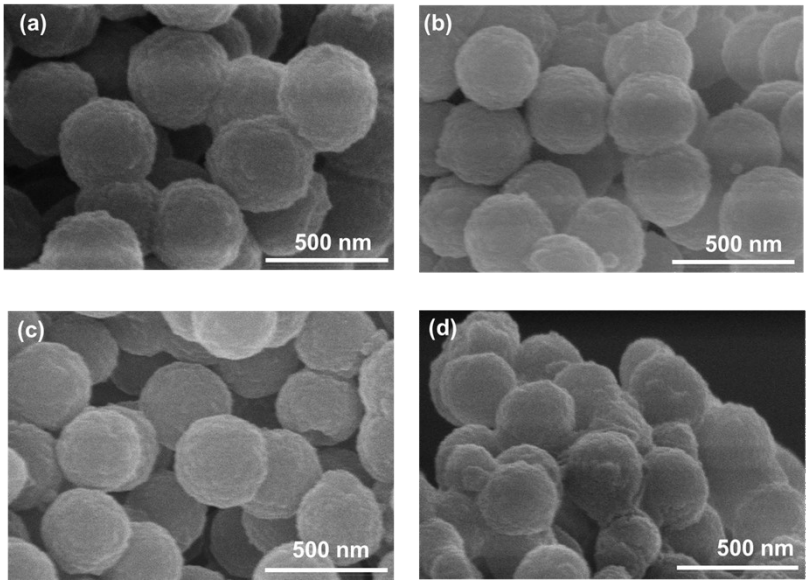


**Fig. S1.** (a-d) Scanning electron microscope images of $HCNS_{G10}$, $HCNS_{G20}$, $HCNS_{G50}$, $HCNS_{G80}$.

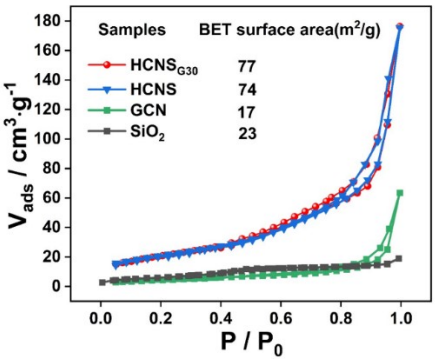


**Fig. S2.** Nitrogen adsorption-desorption isotherms of $SiO_2$, GCN, HCNS $HCNS_{G30}$

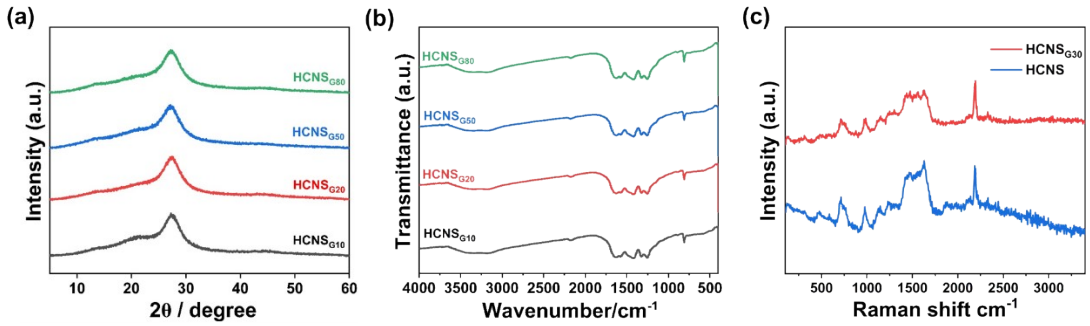


**Fig. S3.** (a) The XRD patterns of $HCNS_{Gx}$. (b) The Ft-IR patterns of $HCNS_{Gx}$. (c) The Raman patterns of HCNS and $HCNS_{G30}$.

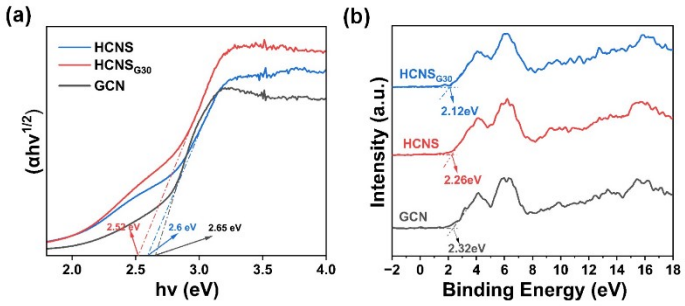


**Fig. S4.** (a) The band gap energy of GCN, HCNS, HCNS$_{G30}$. (b) Valence band X-ray photoelectron spectroscopy.

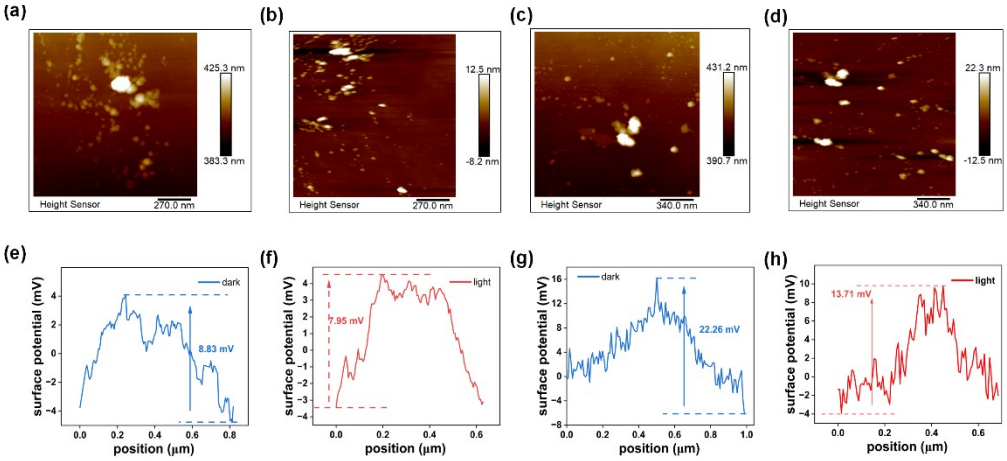


**Fig S5.** KPFM images of, HCNS under (a) darkness and (b) 400 nm LED illumination, HCNS$_{G30}$ under (c) darkness and (d) 400 nm LED illumination. and their corresponding potential diagrams (e-h).

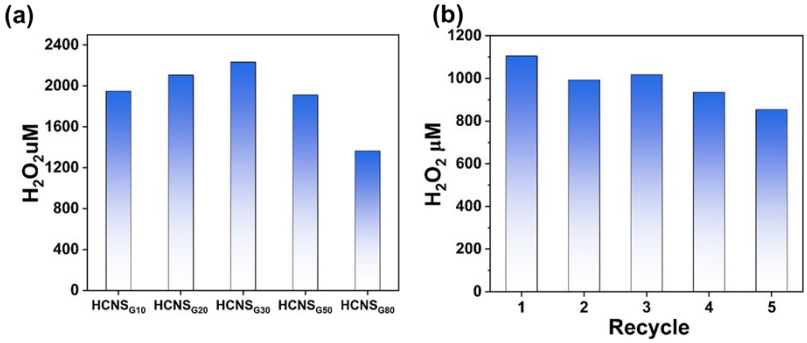


**Fig. S6.** (a) Photocatalytic $H_2O_2$ yields of HCNS$_{Gx}$ (x = 0, 10, 20, 30, 50, 80). (b) Stability test of the photocatalytic $H_2O_2$ production reaction of HCNS$_{G30}$.

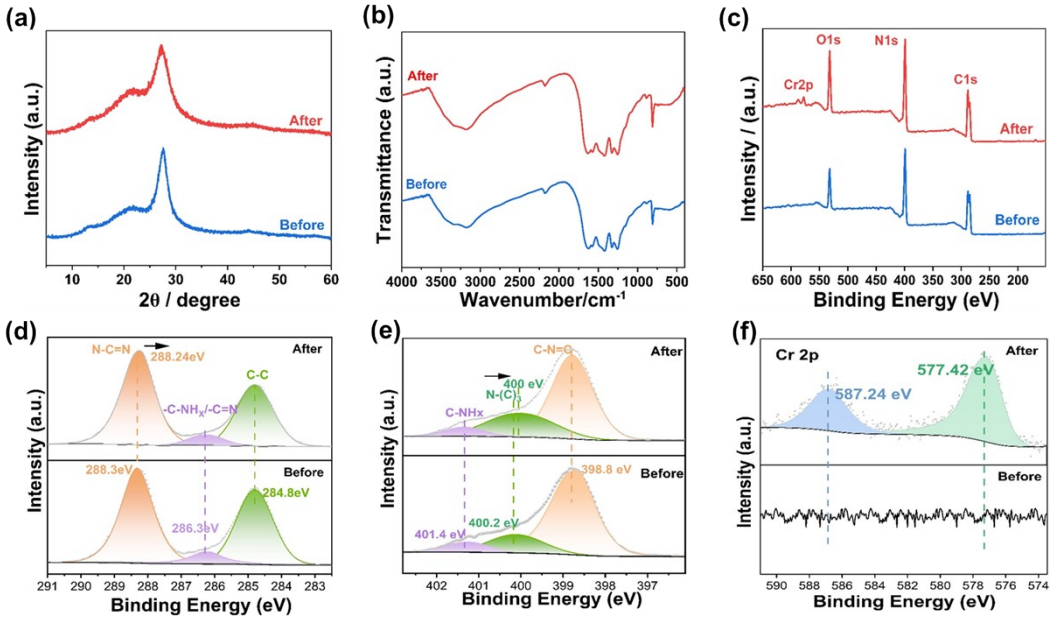


**Fig. S7.** The patterns of $HCNS_{G30}$ before and after the reaction (a) XRD, (b) Ft-IR. (c) Survey XPS spectra, High-resolution XPS of (d) C1 s, (e) N1 s, (f) Cr2p of $HCNS_{G30}$ before and after the reaction.

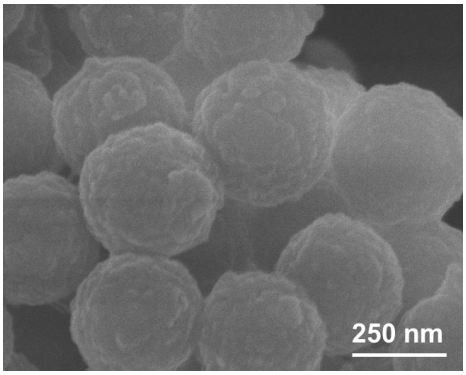


**Fig. S8.** The SEM image of $HCNS_{G30}$ after the reaction.

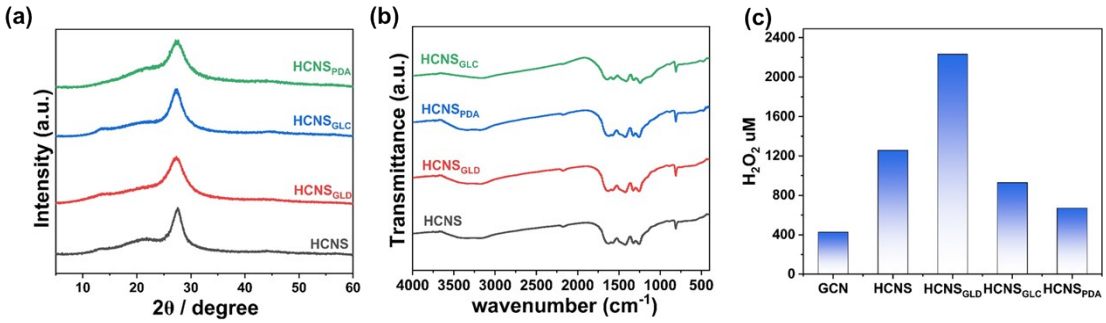


**Fig. S9.** (a) The XRD pattern and (b) FT-IR spectra of different monomers of its C content. (c) Photocatalytic $H_2O_2$ yields of different monomers of its C content.

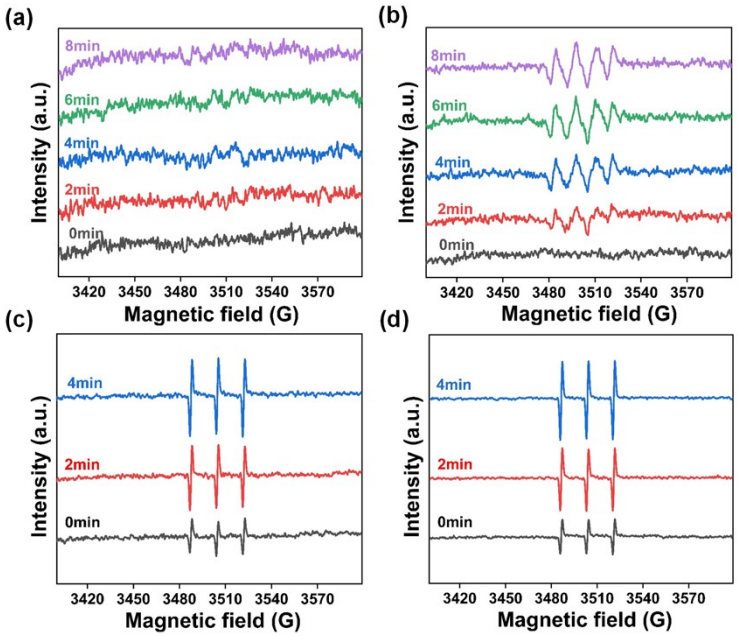


**Fig. S10.** Photocatalytic production of $H_2O_2$ mechanism study, superoxide radicals trapped by DMPO of (a) HCNS, (b) $HCNS_{G30}$, singlet oxygen trapped by TEMP of (c) HCNS, (d) $HCNS_{G30}$.

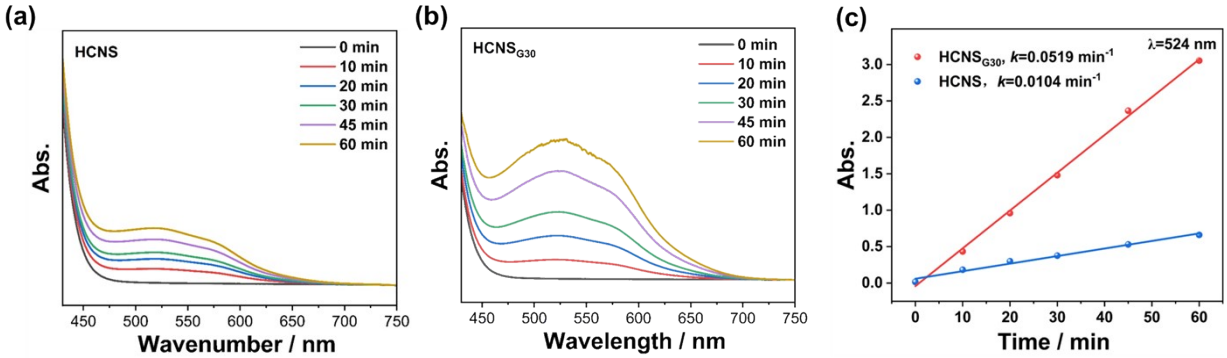


**Fig. S11** UV–vis absorption spectra of the NBT solution with the presence of (a) HCNS, (b) $HCNS_{G30}$ under the light irradiation. (c) UV–vis absorption spectra (524nm) of the NBT solution with the presence of HCNS and $HCNS_{G30}$ under the light irradiation.

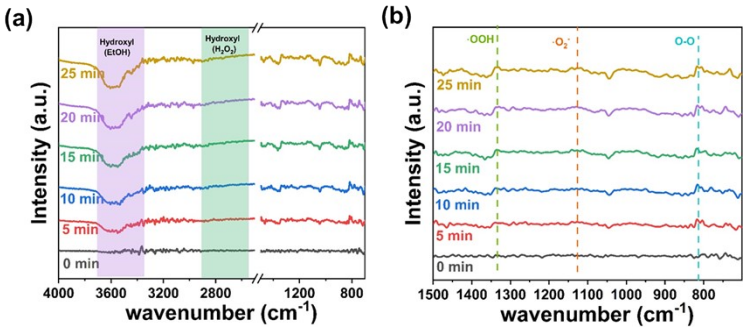


**Fig. S12** The *in-situ* DRIFT spectra of the HCNS for, (a) full spectrum (4000-700cm$^{-1}$), (b) the spectrum from 1500-700cm$^{-1}$.

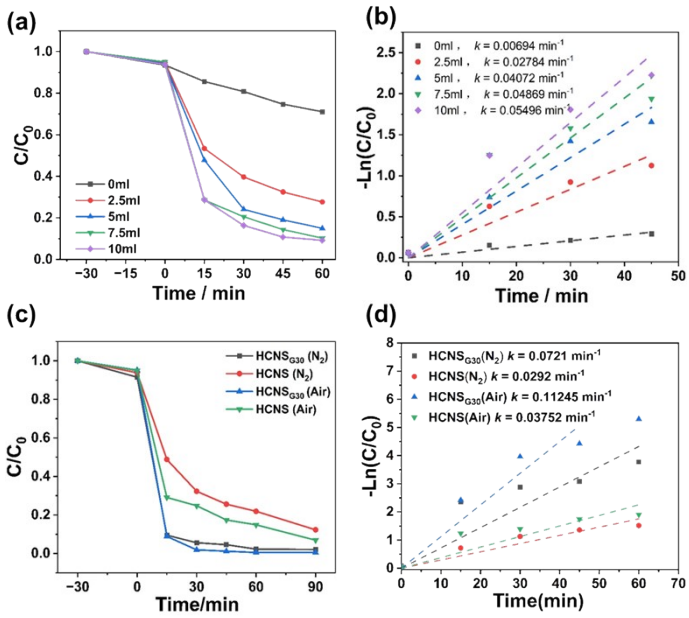


**Fig. S13**. (a) Photocatalytic reduction rates of Cr (VI) by $HCNS_{G30}$ under diverse content of hole scavenger. (b) First-order reaction kinetics of photocatalytic reduction of Cr (VI) by $HCNS_{G30}$ under diverse content of hole scavenger. (c) photocatalytic reduction rates of Cr (VI) by HCNS and $HCNS_{G30}$ under diverse atmospheres, (d) First-order reaction kinetics of photocatalytic reduction of Cr (VI) by HCNS and $HCNS_{G30}$ under nitrogen and air conditions.

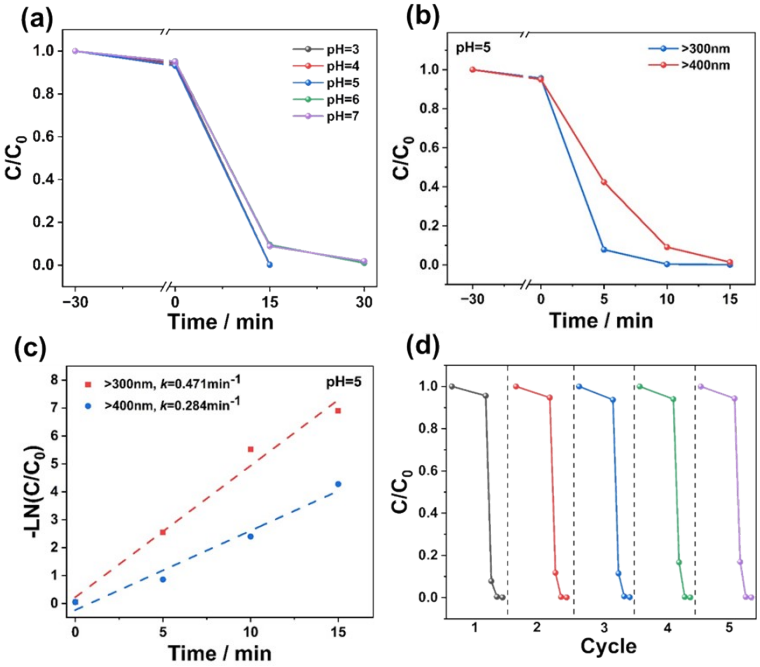


**Fig. S14**. (a) Photocatalytic reduction rates of Cr (VI) by $HCNS_{G30}$ under diverse pH. (b) photocatalytic reduction rates of Cr (VI) by HCNS and $HCNS_{G30}$ under diverse light intensity, (c) First-order reaction kinetics of photocatalytic reduction of Cr (VI) by HCNS and $HCNS_{G30}$ under diverse light intensity. (d) Stability test of the photocatalytic Cr(VI) reduction reaction of $HCNS_{G30}$.

1. S. Samanta, R. Yadav, A. Kumar, A. Kumar Sinha and R. Srivastava, *Applied Catalysis B: Environmental*, 2019, **259**, 118054.
2. X. Dang, X. Cui, H. Zhang, X. Chen and H. Zhao, *ACS Sustainable Chemistry & Engineering*, 2023, **11**, 13096-13107.
3. T. Li, X. Zhang, C. Hu, X. Li, P. Zhang and Z. Chen, *Journal of Environmental Chemical Engineering*, 2022, **10**(3), 107116.
4. N. A. Nordin, M. A. Mohamed, N. S. N. Hasnan, S. F. M. Yusoff, M. S. Mastuli, T. Sugiura and K. Manseki, *Journal of Sol-Gel Science and Technology*, 2024: 1-20.
5. Z. Zhang, P. Luo, L. Gan, Y. Zhao, X. Wang, H. Peng and J. Peng, *Applied Surface Science*, 2024, **649**, 159118.
6. N. A. Nordin, M. A. Mohamed, M. S. Mastuli, S. F. Mohd Yusoff, T. Sugiura and K. Manseki, *Journal of Industrial and Engineering Chemistry*, 2024, **135**, 197-212.
7. N. S. N. Hasnan, M. A. Mohamed, N. A. Nordin, W. N. R. Wan Ishak and M. B. Kassim, *Carbohydrate Polymers*, 2023, **317**, 121096.
8. J. Chen, W. Gao, Y. Lu, F. Ye, S. Huang, Y. Peng, X. Yang, Y. Cai, J. Qu and J. Hu, *ACS Applied Nano Materials*, 2023, **6**, 3927-3935.
9. Q. Jiang, H. Sun, S. Zhou, C. Liu, Z. Zhang, H. Hu, H. Xie, C. Li, Z. Wei and Y. Kong, *Journal of Alloys and Compounds*, 2023, **947**, 169469.
10. C. Liang, M. Cui, W. Zhao, L. Dong, S. Ma, X. Liu, D. Wang, Z. Jiang and F. Wang, *Chemosphere*, 2022, **305**, 135315.
11. M. Murugalakshmi, G. Mamba and V. Muthuraj, *Applied Surface Science*, 2020, **527**, 146890.
12. J. Ye, J. Liu, Z. Huang, S. Wu, X. Dai, L. Zhang and L. Cui, *Chemosphere*, 2019, **227**, 505-513.
13. S. Wang, X. Zhao, H. Muhammad Adeel Sharif, Z. Chen, Y. Chen, B. Zhou, K. Xiao, B. Yang and Q. Duan, *Chemical Engineering Journal*, 2021, **406**, 126849.
14. X. Ma, Z. Zhang, C. Yu, Q. Fan and L. Wei, *Materials Research Bulletin*, 2020, **129**, 110909.
15. A. Meng, W. Tian, H. Yang, X. Wang, X. Wang and Z. Li, *Journal of Hazardous Materials*, 2021, **413**, 125400.
16. M. Saha, S. Ghosh and S. K. De, *Catalysis Today*, 2020, **340**, 253-267.
17. L. Zhang, P. Li, L. Feng, X. Chen, J. Jiang, S. Zhang, A. Zhang, G. Chen and H. Wang, *Chemical Engineering Journal*, 2020, **397**, 129519.
18. Y. Zhang and S.-J. Park, *Applied Catalysis B: Environmental*, 2019, **240**, 92-101.
19. W. Huang, N. Liu, X. Zhang, M. Wu and L. Tang, *Applied Surface Science*, 2017, **425**, 107-116.